ENCIT 2018

ABCM Associação Brasileira de Engenharia e Ciências Mecânicas

17th Brazilian Congress of Thermal Sciences and Engineering
November 25th-28th, 2018, Águas de Lindóia, SP, Brazil

ENCIT-2018-0656
On the synthesis of the transfer matrix of thermoacoustic cores from arbitrary engine performance

Denis Leite Gomes[†]
Flávio de Campos Bannwart[‡]
University of Campinas (UNICAMP), School of Mechanical Engineering, Department of Energy, Rua Mendeleyev, 200, CEP 13083-860, Cidade Universitária "Zeferino Vaz", Campinas/SP, Brazil
[†]denisleitegomes@gmail.com, [‡]fcbannwart@fem.unicamp.br

Abstract. *Thermoacoustic engines convert thermal into mechanical energy by means of spontaneous acoustic oscillations in a working gas confined within a tubular network, whose configuration may lead to either standing or traveling waves. Its main segment is the thermoacoustic core (TAC), defined as the waveguide interval where the temperature gradient is inhomogeneous and, if sufficiently high, generates the acoustic field. The thermoacoustic phenomenon occurs within the open pores of its main component: stack or regenerator. From the transfer matrix of the TAC filled with a specific porous material, different engines can be designed by varying the lengths of the other waveguide segments, and their energetic performances estimated. Therefore, an optimization can be carried out by pursuing the best waveguide configuration for each TAC. However, such procedures may be time-demanding as they follow a forward problem for each sample of porous material under investigation, and the chances of achieving a good TAC design may not be favored in this trial and error process. As an attempt to improve the criteria for porous material selection, we explore in this work an inverse problem: the synthesis of the TAC transfer matrix from an arbitrary engine performance. Previous experimental data from TACs of two different porous materials are analyzed for a standing wave engine configuration. Each transfer coefficient is disturbed in both amplitude and phase in simulations so that to evaluate the effects on the thermoacoustic gain. The resulting artificial matrices lead to better energetic performances and rise discussions toward the feasibility of the corresponding porous materials.*

Keywords: *thermoacoustics, transfer matrix, thermoacoustic core, inverse problem, thermoacoustic engine.*

1. INTRODUCTION

Thermoacoustics concerns the interplay between heat and acoustic oscillations which take place in fluids flowing over solid substrates. The first recorded observation of sound generation due to heat transfer seems to be that of a Buddhist monk who "reported the loud tone radiated by a ceremonial rice-cooker in his diary, in 1568" (Noda and Ueda, 2013). Nevertheless, the same event has been associated with the use of the glassblowing technique, whose development dates back to the 1st century BC. However, the first formal record of the phenomenon of oscillations caused by heat conduction into partially confined gases was conducted in 1777 by Higgins, who investigated the influence of the positioning of a hydrogen diffusion flame inside a large pipe when producing what he called "singing-flame oscillations" (Higgins, 1802). Based on a similar effect that glassblowers reported as a loud and monotonic sound produced when connecting a thin cold tube to a molten glass bulb, Sondhauss conceived what is considered the precursor of a thermoacoustic engine (Avent and Bowen, 2015). It was only by the end of the same century that the first qualitative description of sound vibrations maintained by heat was given by Lord Rayleigh (1896). The first consistent analytical description of the phenomenon were layed down by Rott (1980), who presented its Rott (1969), coined as *Thermoacoustics* in Rott (1980). In the eighties, Gregory W. Swift and fellows at Los Alamos National Laboratory extended this work developing several configurations of resonator networks to build and explore engines and refrigerators (Swift, 2002).

Thermoacoustic devices are categorized according to the direction of the heat flow. When heat flows from a high-temperature source to a low-temperature sink, producing acoustic power, they are designated thermoacoustic engines. Conversely, when acoustic power is consumed to transport heat from a low-temperature source to a high-temperature sink, they are then denominated thermoacoustic heat pumps or refrigerators, depending whether the goal is heating or cooling. Essentially, such devices consist of a network of acoustic resonators inside which a porous material is placed (Bannwart and Arruda, 2009). The mean hydraulic radius of the open pores of this material determines the type of wave that may travel through the device, as it regulates the heat coupling between the gas and the surrounding walls, setting the thermodynamic cycle executed by the oscillating gas parcels (Bannwart *et al.*, 2012). If the characteristic dimension of the pores is of the order of the thermal boundary layer thickness or much smaller than it, respectively, standing waves or traveling waves are formed within the device. The latter is then said to be, respectively, stack-based or regenerator-based.

For further understanding, a guide to some of the most important literature available was compiled by Garrett (2003).

Currently there is a growing demand for improving the efficiency of automobiles and cooling machines while reducing their overall environmental impact, as they account for a large fraction of the total pollutant emissions (Junior *et al.*, 2017). Thermoacoustic devices may be such a clean technology option as they benefit from the use of inert gases as working fluids and achieve "a substantial fraction of Carnot's efficiency" (Swift, 1988). Thus they are not fossil-fuel based neither contain any toxic substances while achieving a reasonable performance. Also, their construction is simple and they have no moving parts, which contributes to lower costs, higher reliability and almost maintenance-free operation (Arafa *et al.*, 2011). Besides, the operation of thermoacoustic devices does not rely on phase changes, as many conventional thermodynamic cyclic machines do. Hence, they are able to work over a wide range of temperature conditions. Despite this versatility, still none of these devices based on waste heat recovery has become competitive enough to be commercialized (Gardner and Howard, 2009). Although the current devices display modest powers (of the order of a few kilowatts), their power density can be magnified by increasing the pressure amplitude, which in turn raises the interactions of wave harmonics that impair this improvement. Nonetheless, there is still room for the efficiency of such devices to grow as the understanding of these complex nonlinear phenomena increases.

Thermoacoustic engines (TAEs) can be designed numerically, by integration of Rott's linear wave equation, for which there are a few software applications available, or analytically, but only for the case of simple waveguide geometries and regular pore structures. Another approach recently employed to the design of TAEs consists on the experimental characterization of the thermoacoustic core (TAC), which is, by definition, the waveguide segment where the temperature gradient is inhomogeneous. The TAC is the most critical element of such engines and therefore this method is very useful for determining the best-performing porous material. However, such procedures may be very time demanding and their performance can only be determined after the TAC definition.

As an attempt to improve the criteria for a priori porous material selection, we investigate in this work an inverse problem: the synthesis of the TAC transfer matrix ($\mathbf{T}_{TAC}$-matrix) from an arbitrary engine performance, which would be guided according to specific boundary conditions and energy availability. Although regenerator-based (or traveling wave) devices are usually more efficient than stack-based (or standing wave) ones, they require more complicated design, reason why a standing wave engine was chosen to be studied herein (Poese, 2017). From the resulting artificial $\mathbf{T}_{TAC}$-matrix, geometrical parameters (such as porosity, average pore radius and tortuosity) and thermal properties (such as heat exchange coefficients) of its hypothetical porous material can be estimated by solving another inverse problem, as previously done by Guédra *et al.* (2015). Thus, the $\mathbf{T}_{TAC}$-matrix synthesis unfolds as a propitious path to setting up a TAE with a desired arbitrary efficiency.

2. METHODOLOGY

2.1 TAE and TACs under study

A representative scheme of the TAE under consideration is given by Fig. 1. It is formed of a TAC enclosed at both of its sides by two straight waveguides of equal diameter ($d_w = 0.0338$ m). The main constituent of a TAC is the porous material, designated stack for standing wave engines. The stack is essentially an arrangement of open pores wherein self-sustained acoustic oscillations are excited due to a sufficiently high temperature gradient along its longitudinal direction, which is imposed by the hot heat exchanger (HHX) and the left ambient heat exchanger (AHX). This thermal domain is known as the active part of the TAC. Next to it, the passive part, comprising a thermal buffer tube (TBT) and the right AHX, which acts as a heat insulator by a smooth temperature profile decreasing to ambient temperature. Albeit not essential, the TBT assures the TAC may be inserted into any device while prevent preventing alterations to the theoretical T-matrix of the resonator that will follow it. The engine is closed at its extreme right position (x_L) by a rigid wall of infinite impedance ($Z_L \to \infty$) which will reflect impinging waves and cause them to interact with incident waves in a constructive pattern, thereby yielding a standing wave pattern whose length equals a half wavelength of the first mode resonance frequency of the apparatus.

The inhomogeneous temperature triggers the thermoacoustic phenomena, for the standing wave case, when its gradient is steep enough to promote intrinsically imperfect thermal coupling between the acoustic gas parcel and the pore internal walls (Bannwart and Arruda, 2009), surpassing the inherent viscothermal losses. The resulting acoustic power can be harnessed by means of an acoustic load (Z_{load}) at the entrance of the apparatus. However, in virtue of the unknown thermophysical properties and complex geometry of the porous material, describing the temperature field of a TAC is rather complicated and, therefore, also the mathematical model for sound propagation through it. Thus, for simplifying purposes, we assume this temperature profile as linear and choose a blackbox model of the engine constituents in the form of transfer matrices, as described in Section 2.2.

The present work continues the works of Bannwart (2014) by analyzing calculated engines incorporating TACs of constant length ($L_T = 0.46\ m$) for two different porous samples - a Nichrome (NiCr) foam and a Ceramic Catalyst (CCat) - under several operating conditions. The transfer matrices of these TACs ($\mathbf{T}_{TAC}(\omega, \dot{Q}_H)$) were measured as a function of the angular frequency (ω), by steps of 1 Hz within the interval of 30 to 250 Hz, as well as the heat power supply

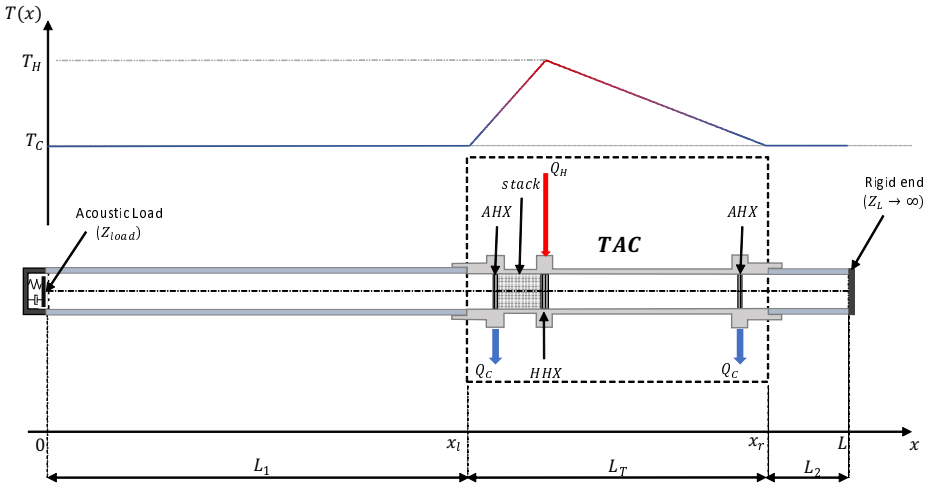

Figure 1: Sketch of the studied TAE. The left and right ends of the TAC are represented by $x_{l,r}$ while those of the TAE are designated by $x_{0,L}$. Adapted from Bannwart (2014).

$\dot{Q}_H$, which was provided to the HHX from 0 W to 81 W by steps of 9 W. All TAEs were designed by first varying the waveguide at left within the ranges of $1.0 \leq L_1 \leq 4.2$ in 80 equally spaced steps for NiCr foam TACs (NiCr TACs) and $0.6 \leq L_1 \leq 4.0$ in 60 equally spaced steps for CCat TACs, and the other in the range $0.0 \leq L_2 \leq 0.4$ in 40 equally spaced steps for both of them. These intervals and increments were chosen such that the best sets of optimized engines would be contemplated along with the descending surface that portrays a steep decline in performance, signaling prohibitive design configurations. A detailed description of the experimental setup in addition to information on the characterization and designing procedures of the optimization are given in his thesis.

2.2 Transfer matrix content

A one dimensional two-port network can be represented by sequential transfer matrices of four coefficients, one matrix for each segment. In our case, the waveguide is subdivided in three segments, being the TAC the central on. Once experimentally characterized, the inner features of the TAC may not be relevant. So employing transfer matrix suits well in some thermoacoustic applications because of the difficult fluid-dynamic description through complex porous materials may be avoided, as demonstrated by (Bannwart *et al.*, 2013). For the other two segments, simple in geometry and constitution, the wave propagation is analytically described in T-matrices as shown in Eq. 1. Thus, provided the transfer matrix, the acoustic field (complex pressure, $\tilde{p}$, and volume velocity, $\tilde{u}$) at the exit of a segment can be obtained from its counterpart at the entrance, independently of its complexity (for example, see Eq. 4).

From literature, the T-matrix of a lossy straight waveguide is analytically given by

$$\mathbf{T}_w = \begin{bmatrix} cos(kL_w) & iZ_c sin(kL_w) \\ \frac{i}{Z_c} sin(kL_w) & cos(kL_w) \end{bmatrix}, \tag{1}$$

where $w = 1, 2$ stand for the T-matrices of waveguides L_1 and L_2, respectively, and

$$k = \frac{\omega}{c_0}\sqrt{1 + \frac{f_\nu + (\gamma - 1)f_\kappa}{1 - f_\nu}} \tag{2}$$

is the lossy complex wave number, and

$$Z_c = \rho_0 c_0 / \left[\phi S \sqrt{(1 - f_\nu)[1 + (\gamma - 1)f_\kappa]}\right] \tag{3}$$

stands for the characteristic complex impedance of a duct; c_0 and ρ_0 are, respectively, the adiabatic sound speed and the fluid density at the ambient temperature T_0 (which was around 295.2 K in our case), γ is the ratio of specific heats of the working gas, ϕ is the porosity of the mean cross-sectional area S (i.e., for waveguides, $\phi = 1$), and, finally, f_ν and f_κ are the viscous and thermal functions which take account of the viscous and thermal attenuation effects.

For the case of a TAC transfer matrix, the acoustic field at both sides of the TAC is related by

$$\begin{Bmatrix} \tilde{p}_r \\ \tilde{u}_r \end{Bmatrix} = \mathbf{T}_{TAC}(\omega, \dot{Q}_H) \times \begin{Bmatrix} \tilde{p}_l \\ \tilde{u}_l \end{Bmatrix} = \begin{bmatrix} T_{pp} & T_{pu} \\ T_{up} & T_{uu} \end{bmatrix} \begin{Bmatrix} \tilde{p}_l \\ \tilde{u}_l \end{Bmatrix}, \tag{4}$$

where the coefficients T_{pp}, T_{pu}, T_{up} and T_{uu} depend on the operating frequency and temperature distribution, and are hereafter collectively referred to as T-coefficients along with the $\mathbf{T}_{TAC}$.

2.3 Performance estimation from T matrices

Bannwart *et al.* (2013) characterized different kinds of porous materials, each sample under several heating conditions, by obtaining their $\mathbf{T}_{TAC}$-matrices from acoustic impedance measurements, for which a new method was proposed; they also designed and optimized both standing and traveling wave TAEs using those experimental matrices. All experimental data and corresponding codes used in the present work came originally from the works of Bannwart (2014). As developed in those works, the optimal waveguide configuration (i.e. L_1/L_2) and the respective operating frequency leading to the highest thermoacoustic amplification gain (G) for each TAC can be found as developed below. See Fig. 2 for example.

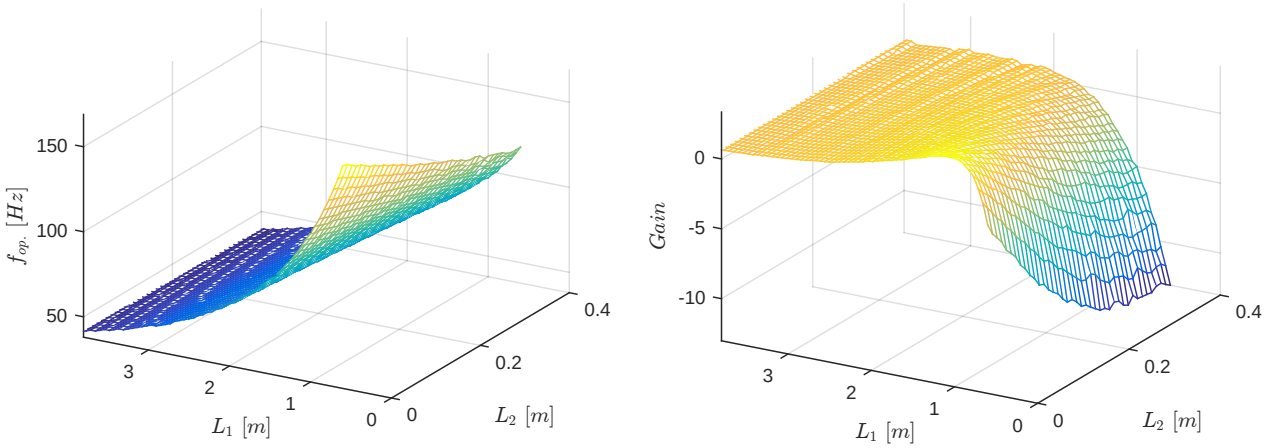

Figure 2: Theoretical operating frequency f_{op} (at left) and gain G (at right) for TAEs at $\dot{Q}_H = 81$ W from measured $\mathbf{T}_{TAC}$ for the Ceramic Catalyst (CCat). Extracted from Bannwart (2014).

The operating frequency of the most unstable mode was obtained for each device from the maximum acoustic impedance at the entrance,

$$\tilde{Z}_0 = \frac{\tilde{p}_0}{\tilde{u}_0} = \frac{\left\{[\mathbf{T}_1 \times \mathbf{T}_{TAC} \times \mathbf{T}_2]^{-1}\right\}_{pp}}{\left\{[\mathbf{T}_1 \times \mathbf{T}_{TAC} \times \mathbf{T}_2]^{-1}\right\}_{up}}, \tag{5}$$

which is useful for predicting the onset of the thermoacoustic instability, i.e., determining its onset conditions (Bannwart *et al.*, 2012). From the knowledge of the experimental T_i-coefficients, the onset conditions required for self-sustained acoustic oscillations can be determined in terms of the thermoacoustic amplification gain,

$$G = \frac{\dot{W}_{TAC}}{\left|\dot{W}_{loss}\right|}, \tag{6}$$

which is a measured of efficiency as it is a ratio between the net acoustic power produced by the TAC,

$$\dot{W}_{TAC} = \left[\frac{1}{2}\,\mathrm{Re}\{\tilde{p}_r\tilde{u}_r^*\} - \frac{1}{2}\,\mathrm{Re}\{\tilde{p}_l\tilde{u}_l^*\}\right], \tag{7}$$

and the overall dissipated power along L_1 and L_2 (the rest of the engine),

$$\dot{W}_{loss} = \left[\frac{1}{2}\,\mathrm{Re}\{\tilde{p}_l\tilde{u}_l^*\} - \frac{1}{2}\,\mathrm{Re}\{\tilde{p}_0\tilde{u}_0^*\}\right] + \left[\frac{1}{2}\,\mathrm{Re}\{\tilde{p}_L\tilde{u}_L^*\} - \frac{1}{2}\,\mathrm{Re}\{\tilde{p}_r\tilde{u}_r^*\}\right]. \tag{8}$$

From that point we introduce a simplified expression for the thermal efficiency of the device:

$$\eta = \frac{\dot{W}_{TAC} - |\dot{W}_{loss}|}{\dot{Q}_H} = \frac{\dot{W}_{out}}{\dot{Q}_H}, \tag{9}$$

where $\dot{W}_{out}$ is the output power produced by the engine at $x = 0$.

The simplification comes from the fact that $\dot{Q}_H$ was not the net heat input in the test rig, as there were many heat losses by conduction and natural convection to the laboratory environment. A better modeling would demand to know

the actual temperature profile inside the TAC, which may be inferred by acoustical means besides other data from those works.

To sum up, the T-matrix gives a proportion between the acoustic field at two positions, so power proportions should be constant for an engine operating at different power densities. Thus, gain calculations will not depend on the absolute power of the the engine, allowing Bannwart (2014) to consider a reference pressure amplitude of 1 Pa at its entrance.

3. ANALYSIS AND INVESTIGATION

Our analysis starts from the results, data and computational codes of the optimization process developed in Bannwart (2014). We explore this data generating new comparisons and new perspectives to pursue a realistic synthetic TAC transfer matrix aiming better engine performances.

For the present study, we selected all engines which satisfied the chosen operating frequency of 70 Hz. This amounted to a total number of 251 TAE configurations for CCat TACs and 396 TAE configurations for NiCr TACs.

First, to investigate convenient frequencies, the total length of all designed engines are plotted against their associated frequencies, as shown by Fig. 3. The isolated points above the curve illustrate the TAEs operating at the second resonant

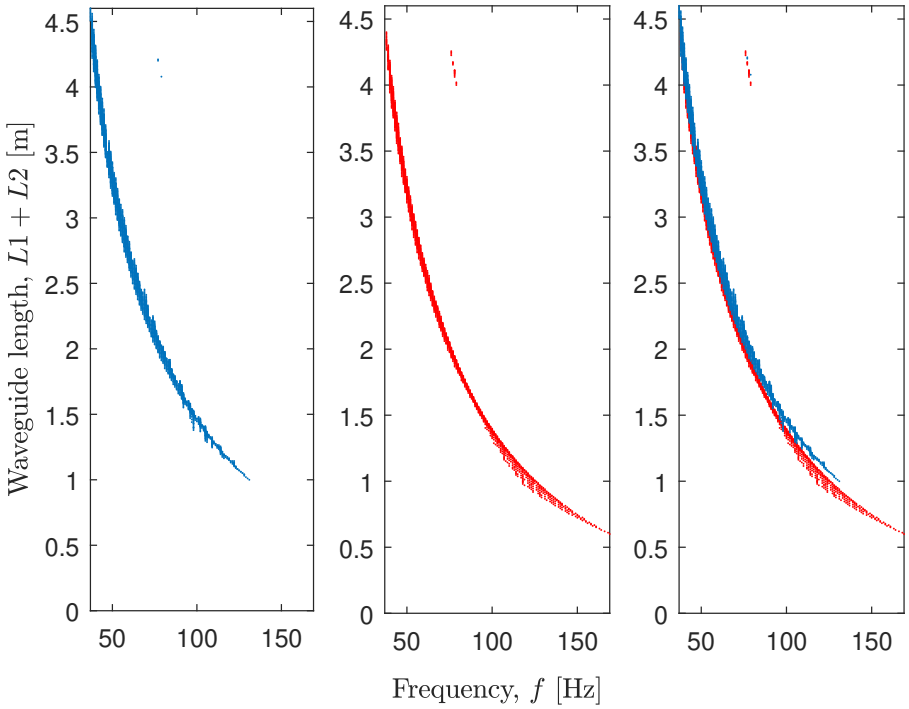

Figure 3: Overall waveguide length for NiCr foam (blue) and CCat (red) TAEs operating at 81 W.

mode and reveal that in such cases the size of the waveguides will have to be much greater than on the first mode for the same heat input regime. Organizing collected data, we observed a trend that as the frequency is increased the number of waveguide combinations that will suit that oscillating mode is decreased. This consequence is manifested by the decreasing density of points at higher frequencies in Fig. 3 for both sets of regenerator-based (blue) and stack-based (red) TAEs.

Engines of different total lengths can result on the same operating frequency due to either the TAC asymmetry, which allows infinite solutions within limited intervals, or to the effect of the rounding applied in the simulation for the determination of the first mode resonance. The latter is a procedure to ensure that the projected waveguides agree with the integer frequencies on which the TAC samples were characterized. The engines were originally evaluated operating at non-integer frequencies utilizing interpolated TAC matrices.

3.1 Influence of the overall waveguide length on the gain

When the selection criterion is based on useful thermodynamic machines ($G > 1$), the overall number of satisfying engines has decreased for the NiCr foam and CCat from 3200 to 2005 and from 2400 to 1978, respectively. For simplicity, the engines operating at the highest heating power supply (81 W) were selected from the previous group of 70 Hz engines, totaling 46 NiCr TAEs and 25 CCat TAEs, and are shown in Fig. 4, which displays their gain. Each dot represents a TAE whose length is given by the sum of the waveguide length ($L_1 + L_2$, restricted to the ranges specified in Section 2.1) with the TAC length (L_T). Clearly, only some CCat TAEs would produce useful acoustic power while all NiCr TAEs would

have the acoustic power produced by the TAC dissipated either within the TAC itself or along the waveguides.

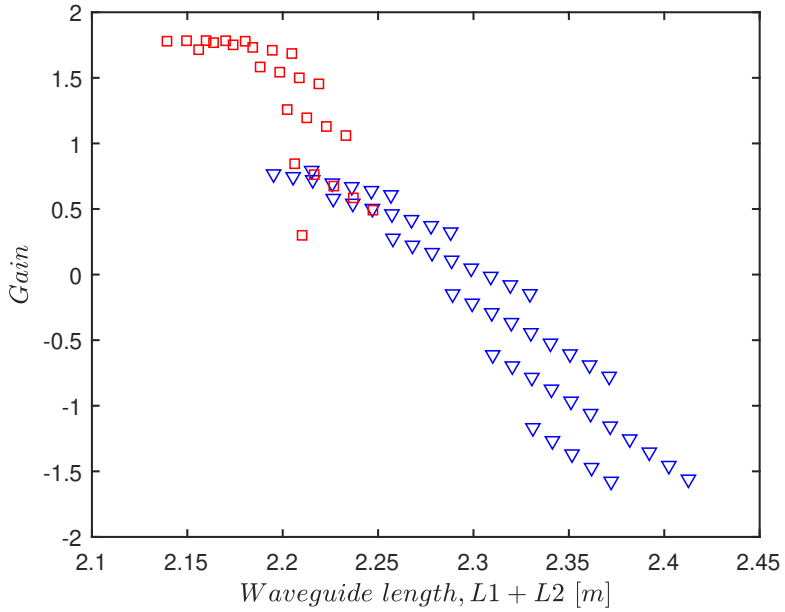

Figure 4: $Gain$ as a function of overall waveguide length for NiCr foam (blue) and CCat (red) TAEs at 70 Hz and 81 W.

From calculated engine data, we observed a pattern that favors those engines with a shorter - and sometimes even null - length of L_2, as L_1 is likewise reduced yet kept long enough to preserve the same desired operating frequency. This underlines what could be inferred by looking at Fig. 4. As can be noticed, G suffers an abrupt decline as the overall waveguide length is increased. Still looking at the same figure, a clear division of the data is perceptible, where groups of points from 4 to 10 elements seem to form consecutive curves that superpose one another as $L_1 + L_2$ becomes lower. These big leaps from one curve pattern to the other are essentially due to changes in L_1, whose step is greater, while the short ones derive from L_2, whose step is smaller.

The best engines, i. e. the ones which have the highest G, tend to be those with a shorter L_2, or even non-existent, in a way that L_1 compensates this reduction, but still allows the engine to operate at the same frequency. This means that the performance is more sensitive to changes on the geometry towards the end of the TAC where the temperature profile is smoother. This suggests that the passive part of the TAC may contribute negatively to the efficiency of the machine. Also, we checked that the longer the waveguides for a certain frequency, the higher the gain, attesting that there is a lower dissipation. This is in accordance with data collected in the optimization process which suggest a growth in the input impedance as the engine size is decreased.

Ideally, to understand how important for the performance is every coefficient, one would like to be able to see its influence on the gain when the heat input is constant and the operating frequency is allowed to vary and vice-versa. Yet it is not possible to keep the same device dimensions, and therefore the same dissipated power, while varying the working frequency because the sound velocity is constant. Consequently, the influence of the frequency is not verified here, as it was done in previous works.

Before moving on with the synthesis, three investigations were carried out so as to evaluate the perspectives for arbitrarily increasing efficiency within acceptable limits by changing each coefficient. In Section 3.2, we analyze how heat input would impact each T_i-coefficient for both TACs. Then, in Section 3.3, we assess the behavior of the gain as each T_i-coefficient is modified. In Section 3.4, we compare transfer matrices of both materials for all heating regimes to choose plausible intervals from a vast range of magnitude and phase values. Finally, transfer matrices were synthesized and evaluated in Section 3.5 as well as an interpretation of the physical aspects that may contribute to the corresponding changes on transfer matrix coefficients.

3.2 Investigating the influence of the heating power supply on the T_i-coefficients

In virtue of the very different nature of both materials (the firt, metalic, and the latter, refractory), their temperature profiles are considerably different as well as the sound speed. Thus, waveguide lengths for these TACs are different for a constant operating frequency, what made it prohibitive to find engines of both sample materials which would have the same size while operating at the same conditions. Nor is it possible to find similar configurations which lead to the greatest number of heating regimes for both TACs. As a consequence, two TAE configurations which satisfied the greatest number of possible heating regimes at 70 Hz were chosen, namely $L1 = 2.1342$ m and $L2 = 0.0923$ m ($L_1 + L_2 = 2.2265$ m) for the NiCr TAC and $L_1 = 2.0983$ m and $L_2 = 0.0410$ m ($L_1 + L_2 = 2.1393$ m) for the CCat TAC.

The dependence of the magnitude of the T_i-coefficients with the heating power supply ($\dot{Q}_H$) is shown in a relative scale in Fig. 5, where the off-diagonal components are represented non-dimensionalized by the characteristic complex impedance of the waveguides, Z_c, given by Eq. 3.

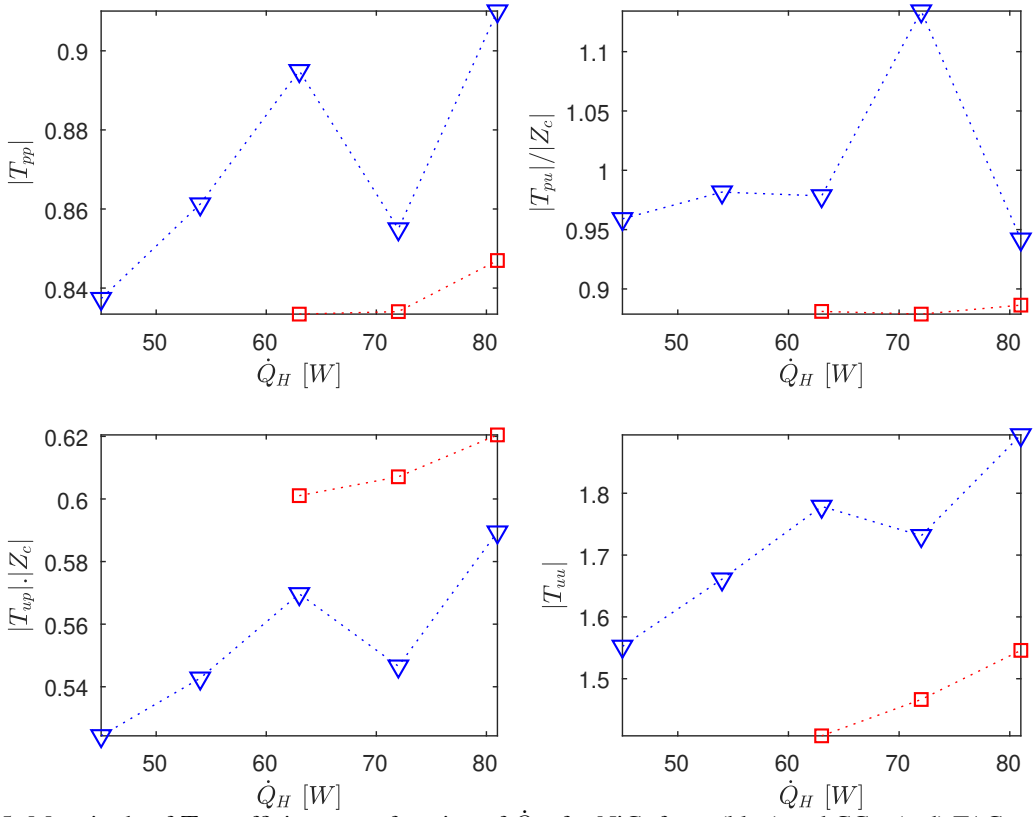

Figure 5: Magnitude of T_i-coefficients as a function of $\dot{Q}_H$ for NiCr foam (blue) and CCat (red) TACs at 70 Hz.

As expected, an overall growing trend is observed in all coefficients as more heat is added to both TACs tested. By comparing both materials in this plot, knowing a priori that the CCat delivers a higher gain for this TAE, one could speculate that a higher $|T_{up}|$ and a lower magnitude of the other three coefficients are responsible for a more efficient TAC. Still, it is visible that $|T_{uu}|$ is the one which has the highest increase with respect to its original value. A local decent is observed between 63 W and 72 W in the NiCr foam sample for all coefficients, except for T_{up}. This coefficient apparently has an opposite behavior than the other ones for NiCr TACs from 54 W on, which is indicative of the underlying interrelation between the coefficients of the transfer matrix, as it already encompasses thermoacoustic non-linearities.

Similarly, Fig. 6 displays the results of this analysis for the phase of the T_i-coefficients in degrees. In this case, the evolution of the coefficients is not so evident for all of them, though one can check out that the ones related to the input volume velocity, i.e. $arg(T_{pp})$ and $arg(T_{up})$, for each respective material have an analogous growing pattern. The same happens to those related to the input pressure $arg(T_{pp})$ and $arg(T_{up})$. However, the latter ones do not always increase. Still, one could guess that a lower $arg(T_{up})$ and a higher phase of the other three coefficients could increase the performance of the TAC. The contrary modifications would probably degrade efficiency. It is interesting to notice that, as with $|T_{uu}|$, $arg(T_{uu})$ is the coefficient whose phase showed the highest increase with respect to its original value.

From a broader point of view, one could judge that a higher heat supply would cause the amplitude of the acoustic field variables to be amplified when passing through the TAC, for the same configuration and input field. However, this cogitation is not always true, as attested by Fig. 7, where the gain increases steadily for CCat but has a slight oscillation for NiCr foam, in the same manner as identified previously with its T_i-coefficients.

Though it would be possible to analyze every coefficient in light of the whole heat input variation, a gain comparison would be impossible because there is no configuration which could bear all heating regimes. In spite of that, we have tested more similar waveguide configurations which did not show much difference in terms of how the heating power supply affects the gain. This indicates that the TAC itself has a stronger influence on the gain when the heat input is increased than the waveguide configuration itself, reason why we did additional investigations in Section 3.4.

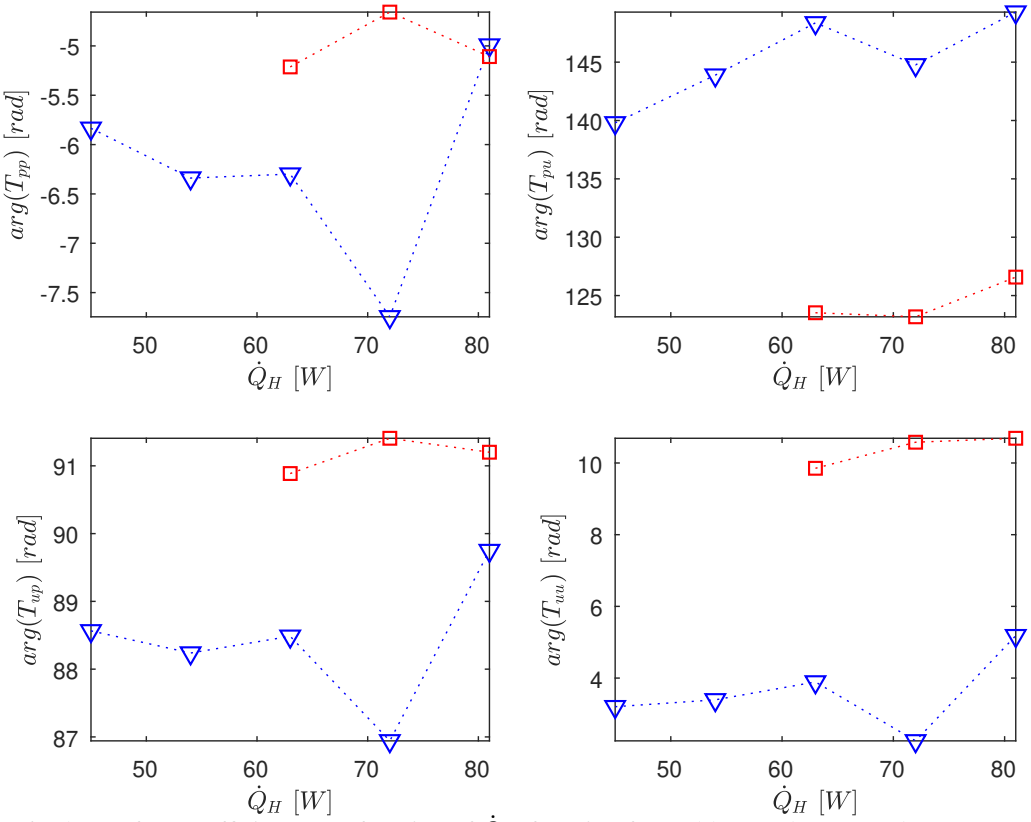

Figure 6: Phase of T_i-coefficients as a function of $\dot{Q}_H$ for NiCr foam (blue) and CCat (red) TACs at 70 Hz.

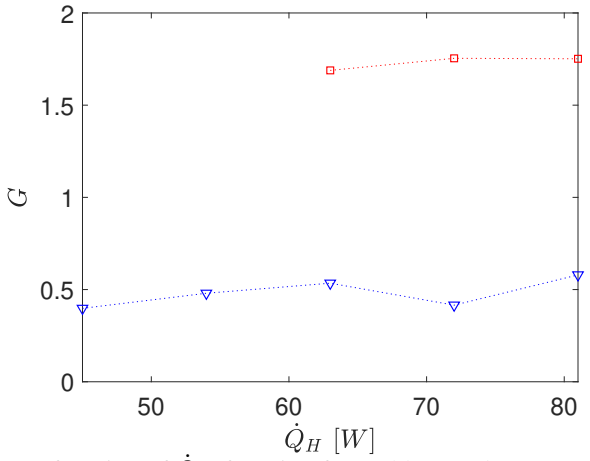

Figure 7: Gain G as a function of $\dot{Q}_H$ for NiCr foam (blue) and CCat (red) TAEs at 70 Hz.

3.3 Investigating the influence of each T_i-coefficient on the gain

We considered a NiCr TAE with waveguide length of 2.2265 m ($L_1 = 2.1342$ m, $L_2 = 0.0923$ m) and a CCat TAE with waveguide length of 2.1804 m ($L_1 = 2.0983$ m, $L_2 = 0.0821$ m) for the present gain calculations. Besides, transfer matrices were evaluated in polar form, respectively, for magnitude and phase changes.

The magnitude of each T_i-coefficient was separately altered by multiplying its original value by a varying *magnitude coefficient* (mc) in a range of 0.5 to 1.5 and the corresponding output gain was computed, as shown in Fig. 8. The black circles represent the original values of the T_i-coefficients. As suggested by the slope of each curve, the gain has an upward trend when $|T_{pp}|$ and $|T_{up}|$ increase. The opposite is also true, so when $|T_{pu}|$ becomes a higher value, while the magnitudes of the other two coefficients become lower, the gain has a downward trend. These results are consonant with what was anticipated in the previous section regarding magnitudes. However, the gain behaves differently for modifications in $|T_{uu}|$ in each material. The NiCr TAC seems to have almost reached a plateau, suggesting that its $|T_{uu}|$ value is almost optimal for the operating conditions considered. On the other hand, the CCat TAC still has room for improvement if $|T_{uu}|$ is diminished.

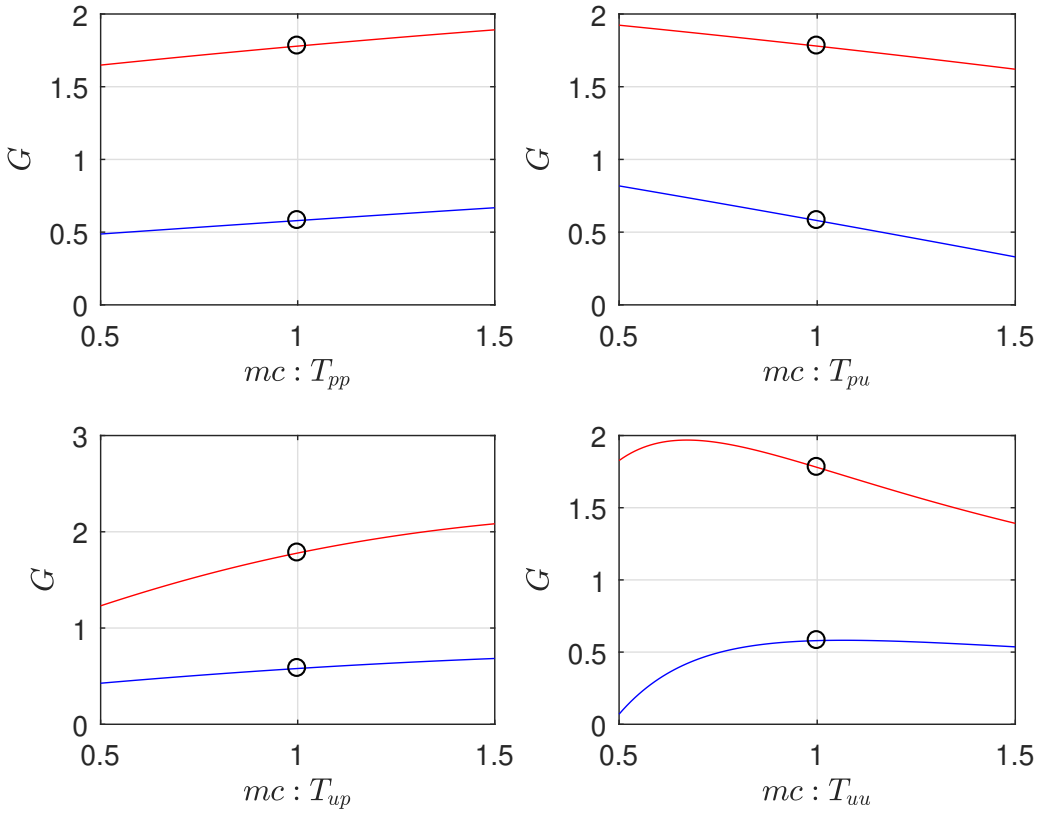

Figure 8: G for magnitude changes of each T_i-coefficient for NiCr foam (blue) and CCat (red) TAEs at 70 Hz and 81 W.

The influence of the phase of each T_i-coefficient was verified by adding to its original value a varying *phase coefficient* (pc) in a range of $-180°$ to $180°$ degrees, respectively corresponding to either delaying or advancing semi-period shifts. The calculated gain results are presented in Fig. 9. Observing the slope of the sinusoidal curves around the original T_i-

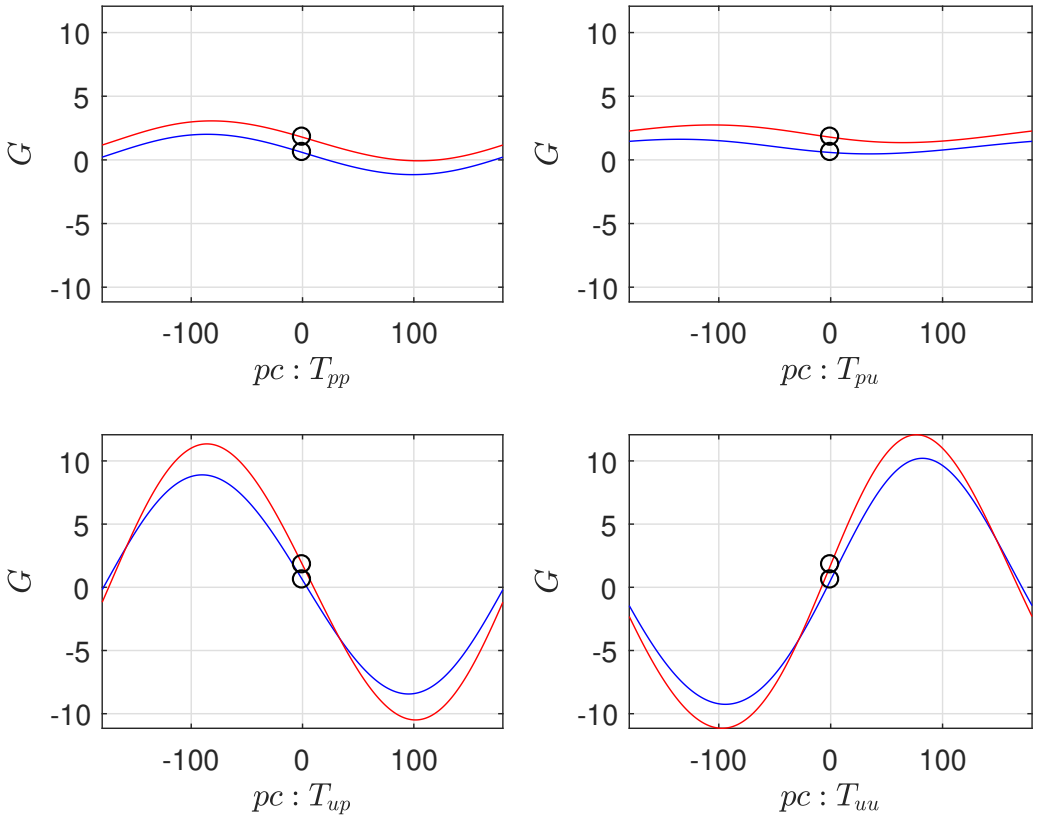

Figure 9: G for phase changes of each T_i-coefficient for NiCr foam (blue) and CCat (red) TAEs at 70 Hz and 81 W.

coefficient values ($pc = 0$), a decrease in efficiency is seen when increasing the phase of all coefficients, except $arg(T_{uu})$. Contrarily, the gain is raised by increasing $arg(T_{uu})$ and decreasing the phase of the other coefficients. Apparently, $arg(T_{uu})$ changes provide the highest gain modifications while $arg(T_{pp})$ and $arg(T_{pu})$ only give modest increments. This suggests that T_{uu} is the coefficient which may provide the most significant contributions to the gain for the same interval of change.

From the analysis above, in principle, one would wish to increase as high as possible $|T_{pp}|$, $|T_{up}|$, $arg(T_{uu})$ at the same time as $|T_{pu}|$, $|T_{uu}|$, $arg(T_{pp})$, $arg(T_{pu})$ and $arg(T_{up})$ are decreased as much as possible. However, such simultaneous edition of the T_i-coefficients would considerably complicate the understanding of how the thermophysical properties of the porous materials affect each coefficient of the transfer matrix.

3.4 Assessment of reasonable coefficient ranges for the synthesis

Despite providing orientations for editing the $\mathbf{T}_{TAC}$-matrix, the investigation of Section 3.3 lacked on reasonable limits for modifying each of the T_i-coefficients in the pursuit of a synthesizable porous material. Thus, we executed an element-wise comparison of the transfer matrix of both materials in each of the heating regimes. This allowed us to prospect a relation between both materials and define a region in the complex domain where the T_i-coefficients of both materials lie, within which the thermal and physical properties of the TACs cause their T_i-coefficient to vary. Through this bounded region, a hypothetical material could be found with intermediate characteristics, ranging from a regenerator-based geometry (such as NiCr foam) to a more stack-based shape (CCat). Before proceeding with this comparison, some geometrical parameters of both porous materials are presented in Tab. 1 and used later for interpreting the differences of both transfer matrices.

Table 1: Geometrical parameters of the porous materials of the characterized TACs from Bannwart (2014).

Material	Radius of the pore (r_p)	Porosity (ϕ)	Free cross-sectional area (S_s)	Tortuosity (α_∞)
NiCr	6.0×10^{-4} m	0.92 ± 0.01 (1)	2.63×10^{-4} m^2 (2)	1.30 ± 0.04 (1)
CCat	5.33×10^{-4} m	0.83	7.45×10^{-4} m^2	1

(1) Parameter estimated in Guédra *et al.* (2015). (2) Parameter calculated from the estimated porosity.

The investigation here was twofold, first for the magnitude, then for the phase, as done in preceding sections. The first range was inspected in the form of a ratio, where the magnitude of each T_i-coefficient of the CCat TAC ($|T_{i_{CCat}}|$) was divided by the magnitude of the corresponding T_i-coefficient of the NiCr TAC ($|T_{i_{NiCr}}|$). The second range inspection was a phase difference, subtracting the phase of each T_i-coefficient of the CCat TAC ($arg(T_{i_{CCat}})$) by the phase of the corresponding T_i-coefficient of the NiCr TAC ($arg(T_{i_{NiCr}})$).

The results of these calculations were summarized, respectively, in Tab. 2 for magnitude ratios, $mr = |T_{i_{CCat}}|/|T_{i_{NiCr}}|$, and in Tab. 3 for phase differences, $pd = arg(T_{i_{CCat}}) - arg(T_{i_{NiCr}})$. These values are employed in the next section for further guidance on the transfer matrix synthesis.

Table 2: Magnitude ratio of each T_i-coefficient of CCat to respective T_i-coefficient of NiCr foam at 70 Hz and $\dot{Q}_H$.

$\frac{\lvert T_{i_{CCat}}\rvert}{\lvert T_{i_{NiCr}}\rvert}$		$\dot{Q}_H$ [W]									
		0	9	18	27	36	45	54	63	72	81
i	pp	1.0039	1.0784	1.0074	1.0221	0.9682	0.9797	0.9584	0.9312	0.9756	0.9307
	pu	0.9070	0.8914	0.9430	0.8109	0.9225	0.8860	0.8896	0.8963	0.7711	0.9366
	up	0.9667	1.1390	1.0893	1.1341	1.0983	1.1210	1.1020	1.0600	1.1160	1.0577
	uu	0.9811	0.8576	0.8026	0.8278	0.8044	0.8205	0.8110	0.7914	0.8470	0.8160

Under ambient condition (0 W), only $|T_{pp}|$ is greater in the CCat TAC ($mr > 1$) while the magnitude of the other coefficients $|T_{i_{CCat}}|$ are lower. With respect to the phase, except for $arg(T_{pu})$, the phases of the other $T_{i_{CCat}}$ coefficients are greater in the CCat TAC ($pd > 0$). At this unheated regime, the relation between the coefficients of these materials is uniquely associated to their geometrical properties. This suggests that the more organized nature of the CCat TAC, i.e. parallel straight pores, may be related to this.

As more heat is added to the TAC, the overall effect is that the magnitude ratio of each coefficient (mr_i) has a decreasing trend, except for the one associated to up (mr_{up}). Regarding the phase difference of the coefficients, pd_i, in general all of them have a tendency to be only slightly decreased, except for the one associated to pu (pd_{pu}), which has a more expressive drop. Comparing both mr and pd from the highest heating power supply to the ambient condition, the

Table 3: Phase difference in degrees between each T_i-coefficient of CCat and respective T_i-coefficient of NiCr foam at 70 Hz and $\dot{Q}_H$.

$arg(T_{i_{CCat}})$ − $arg(T_{i_{NiCr}})$		$\dot{Q}_H$ [W]									
		0	9	18	27	36	45	54	63	72	81
i	pp	2.23	−0.04	0.81	3.84	1.04	1.03	1.36	1.09	3.09	−0.12
	pu	−15.22	−12.82	−19.71	−20.63	−20.83	−19.19	−22.22	−24.84	−21.59	−22.71
	up	1.51	−0.67	0.69	4.34	1.95	2.36	2.64	2.40	4.46	1.45
	uu	7.74	3.02	4.46	8.09	5.85	6.09	6.18	5.96	8.33	5.51

increment of mr_i with respect to their original values (in this case, at 0 W) is about 3% for mr_{pu}, 9% for mr_{up}, while its decrement is approximately 7% for mr_{pp} and 17% for mr_{uu}. In regard to the phase, the decrement of pd_i is around 105% for pd_{pp}, 49% for pd_{pu}, 4% for mr_{up}, while its increment is approximately 29% for mr_{uu}.

Even tough these numbers show some trends for the evolution of the T_i-coefficients, there are some fluctuations in intermediate heating regimes that demonstrate the susceptibility of the measurements to the stabilization of the temperature profile during the measurement of the TAC transfer matrices in the test rig, as evidenced by Fig. 10. This probably

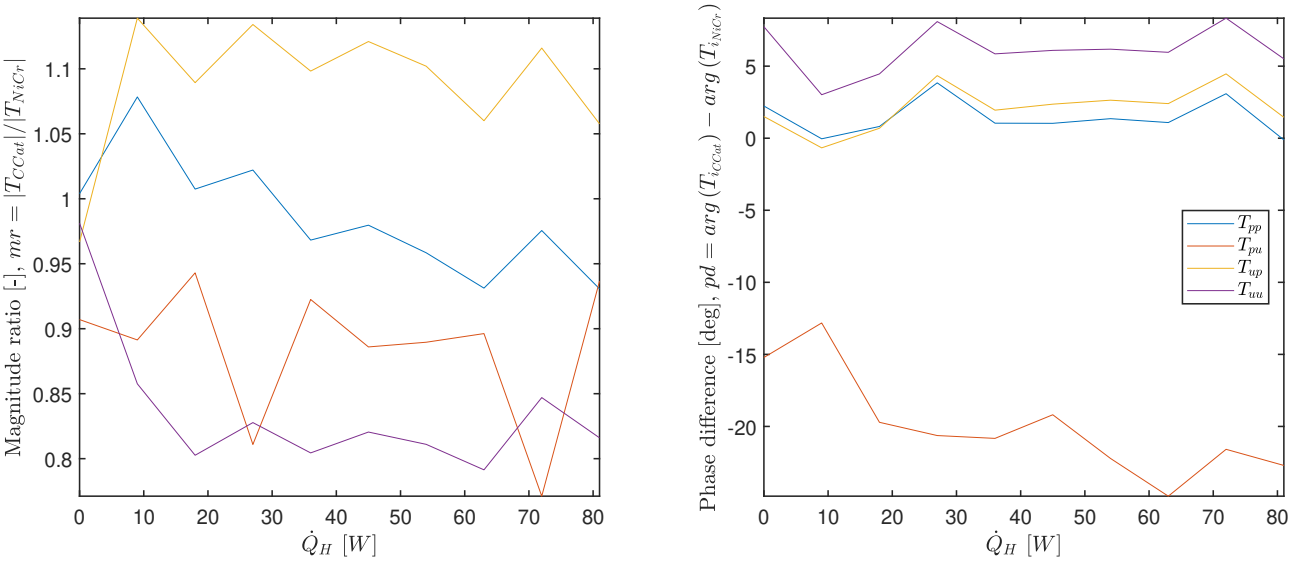

Figure 10: Evolution of the magnitude ratio mr and the phase difference pd between each T_i-coefficient of CCat and NiCr foam at 70 Hz with the heating power supply $\dot{Q}_H$.

happens in virtue of the tortuosity of the open pores of the NiCr TAC, where convection mechanisms are not favored, even with its higher thermal conductivity when compared to that of the CCat TAC. This can also explain the oscillations observed in the figures of Section 3.2 for the NiCr TAC.

Even though the CCat TAC always provides higher gain values (see Fig. 7), only its $|T_{pu}|$ value is usually greater than that of the NiCr TAC for higher heat input values. However, the pd bounces between -1 and 9 repeatedly for the other three coefficients, except for $arg(T_{pu})$, what probably means that the heat input may not have a significant influence on those three. At the same time, the phase difference associated to pu (pd_{pu}) is highly affected by the heating supply. From the parameters studied above, the ones which suffer the most expressive changes with the heating power supply are T_{pu}, with respect to its magnitude, and T_{uu}, with respect to its phase.

3.5 Synthesized matrices

Based on the results of the previous section, we chose to synthesize $\mathbf{T}_{TAC}$-matrices by taking the original CCat transfer matrix (T_{CCat}) and individually editing each of its coefficients in both magnitude and phase. We modified the magnitude of each $T_{i_{CCat}}$ coefficient by multiplying or dividing its original value by mr_i, ensuring that synthesized matrices would necessarily have a greater gain G than the original one. Accordingly, we synthesized eight different $\mathbf{T}_{TAC}$-matrices with arbitrary greater efficiencies for the unheated condition and for the highest heating power supply, as displayed by Fig. 11. The blue line represents the original gain of the CCat TAC at ambient temperature and no heat source. Above them, its respective synthesized $\mathbf{T}_{TAC}$-matrices are shown as blue squares for every T_i-coefficient in magnitude (Fig. 11a) and in phase (Fig. 11b). The red line marks the original gain of the CCat TAC at 81 W, while the red circles above it represent its synthesized $\mathbf{T}_{TAC}$-matrices. The green dashed line stands for the threshold of the

thermoacoustic instability, above which the TAC can produce useful acoustic work. The black line is representative of the limit from which some work is produced but fails to surpass internal losses. An unheated TAC should never trespass this threshold, as there is no power source. Otherwise it would violate energy conservation, as work would be created.

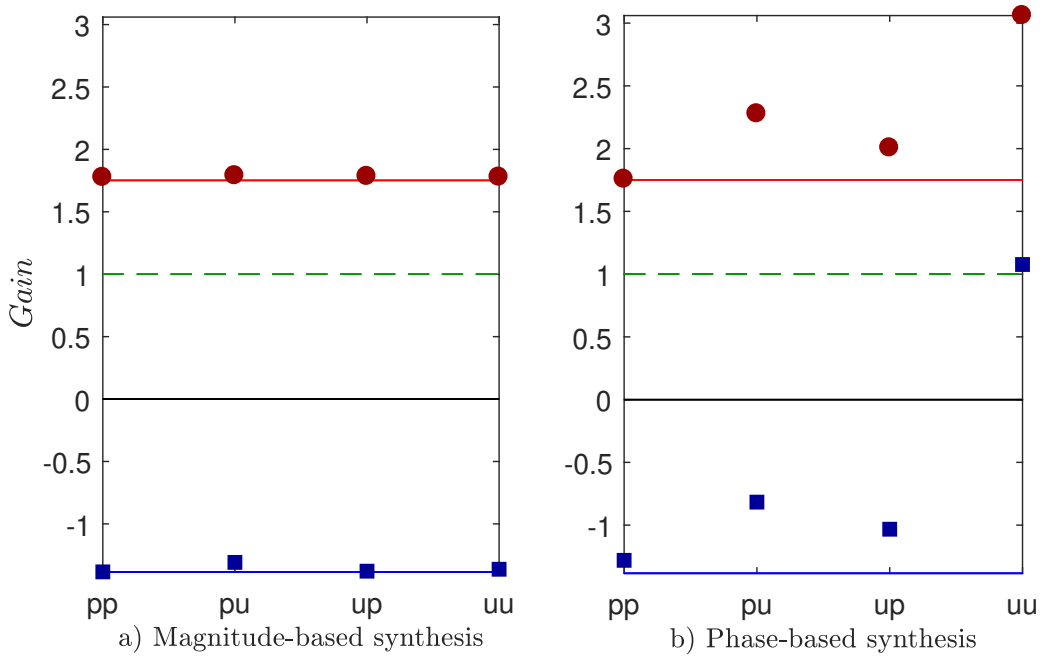

Figure 11: Gain of the synthesized T-matrices at 70 Hz: a) based on the magnitude ratios, and b) based on the phase differences, for the ambient (unheated) condition (blue) and for the heating power supply of 81 W (red).

Examining Fig. 11, it becomes clear that the synthesis based on the phase of T_{uu} has generated an unheated TAC with $G > 1$. From this observation, we can infer that the synthesis has the equivalent effect of simultaneously changing the geometrical properties of the porous material inside the TAC as well as artificially inserting a heating power supply.

Fig. 11 shows that phase-based synthesis of T_{uu} gives the highest arbitrary gain, followed by that of T_{pu}, almost duplicating it. This is an indication of the importance of understanding how this coefficient is influenced by geometrical and thermal properties, specially regarding phase modifications.

For this reason, from Eq. 4, we write the T_i-coefficients in terms of the acoustic field of both sides of the TAC for better understanding the relationship between them:

$$T_{pp} = \frac{1}{\tilde{p}_l}\left(\tilde{p}_r - T_{pu}\tilde{u}_l\right) = \frac{\tilde{p}_r}{\tilde{p}_l} - \frac{1}{Z_l}T_{pu} \tag{10}$$

$$T_{pu} = \frac{1}{\tilde{u}_l}\left(\tilde{p}_r - T_{pp}\tilde{p}_l\right) = \frac{\tilde{p}_r}{\tilde{u}_l} - Z_l T_{pp} \tag{11}$$

$$T_{up} = \frac{1}{\tilde{p}_l}\left(\tilde{u}_r - T_{uu}\tilde{u}_l\right) = \frac{\tilde{u}_r}{\tilde{p}_l} - \frac{1}{Z_l}T_{uu} \tag{12}$$

$$T_{uu} = \frac{1}{\tilde{u}_l}\left(\tilde{u}_r - T_{up}\tilde{p}_l\right) = \frac{\tilde{u}_r}{\tilde{u}_l} - Z_l T_{up} \tag{13}$$

where Z_l is the complex acoustic impedance at $x = x_l$.

The complex coefficient T_{uu} in Eq. 13 establishes the connection between the volume velocity at left and at right of the acoustic element (Gentemann *et al.*, 2003). As a consequence, the synthesis based on the edition of T_{uu} seems to facilitate the acoustic power transmission through the porous material, increasing the net produced power by raising the volume velocity ratio ($\tilde{u}_r/\tilde{u}_l$) across the TAC. It is also affected by variations on T_{up} and grow with increasing impedance at x_l (Z_l). This supports previous observations where TACs with shorter L_2, i.e. lower impedances, usually have higher gains.

From the present work, we notice that the synthesized $\mathbf{T}_{TAC}$-matrices displayed by Fig. 11 must suffer further verifications such as testing the reciprocity of the synthesized transfer matrices, as it is a reference parameter for the case of $\dot{Q}_H = 0$ W. The synthesized $\mathbf{T}_{TAC}$-matrix should have a determinant around 1 in order to check the practicality of an arbitrary TAC transfer matrix by preventing its shift from ambient condition. Nevertheless, the results obtained point out favorable perspectives for a new approach to the design of more efficient TACs and, as a consequence, better performing thermoacoustic engines.

4. CONCLUSIONS

We have investigated the synthesis of arbitrary transfer matrices of thermoacoustic cores (TACs) and studied the influences of each of its respective coefficients on the performance of a thermoacoustic engine (TAE). In this study, we have developed discussions concerning the parameters that positively contribute to the thermoacoustic gain by exploring experimental data from previous works, where TACs were characterized for different porous materials and optimal designs of TAEs were achieved. Our synthesis have started from those matrices, which were then evaluated toward the optimized improvements in the thermoacoustic gain (G).

This process required the selection of an operating condition and an engine design that would suit this choice in conjunction with the characterized TACs. The sensibility of the gain to the T_i-coefficients was evaluated by individually modifying each of them. The domain of evaluation was exploited over an arbitrary range for the complex magnitude and over a complete period for the complex phase. This allowed us to verify the most influent coefficients that would result, artificially, on a greater performance with respect to the original $\mathbf{T}_{TAC}$-matrix. Then a refined range search was done looking for selected parameter changes on those coefficients by comparing TACs with very different internal structures under the same frequency, heat supply and similar engine geometry.

Finally, eight $\mathbf{T}_{TAC}$-matrices were synthesized, one for each of the studied parameters looking for a greater G. A gain-based comparison was carried out for the TAC transfer matrices, from which we found out that the parameters which have a stronger influence on the the performance of a TAC are the magnitude and phase of T_{uu}. We offered some remarks on geometrical and thermal aspects and which could be associated to the modifications made to these transfer matrices, and particularly the this latter coefficient.

An effective artificial way of increasing the efficiency of a thermoacoustic device can be done by focusing on the sole improvement of its central element, the TAC. Its geometric and thermophysical characteristics have a crucial impact on the behavior of the engine, first on the effective transformation of heat into acoustic power and then on the wave propagation through itself. So far as we know, it has been the first case of synthesized transfer matrices, at least in thermoacoustics, providing a promising approach towards designing more efficient TACs and, therefore, increasing the performance of thermoacoustic engines.

Further investigations would be verifying the possibilities of conceiving new porous materials, what could lead to a metamaterial. Important aspects to be considered would be the type of solid macro-structure, thermophysical properties, and pore geometry.

5. ACKNOWLEDGEMENTS

The authors thank CNPq for the financial support granted to the first author (process number 137083/2017-3).

6. REFERENCES

Arafa, N.M., Ibrahim, A.H., Addas, K. and Abdel-Rahman, E., 2011. "Design considerations for thermoacoustic engines for low onset temperature and efficient operation". In *Forum Acusticum*. Aalborg, Denmark, Vol. 27, pp. 961–966.

Avent, A.W. and Bowen, C.R., 2015. "Principles of thermoacoustic energy harvesting". *The European Physical Journal Special Topics*, Vol. 224, No. 14-15, pp. 2967–2992.

Bannwart, F.C. and Arruda, J.R.F., 2009. "Construction of a demonstrative apparatus for the thermoacoustic refrigeration effect". In *Proceedings of the XIII Int. Symposium on Dynamic Problems of Mechanics (DINAME 2009), Angra dos Reis, RJ, Brazil*. March.

Bannwart, F.C., Penelet, G., Lotton, P. and Dalmont, J., 2012. "Methods for transfer matrix evaluation applied to thermoacoustics". In *Acoustics*. April, pp. 3029–3034.

Bannwart, F.C., Penelet, G., Lotton, P. and Dalmont, J., 2013. "Measurements of the impedance matrix of a thermoacoustic core: Applications to the design of thermoacoustic engines". Vol. 133, No. 5, pp. 2650–2660.

Bannwart, F.C., 2014. *Methods for the transfer matrix evaluation of thermoacoustic cores with application to the design of thermoacoustic engines*. Ph.D. thesis, Université du Maine / Unicamp.

Gardner, D.L. and Howard, C.Q., 2009. "Waste-Heat-Driven Thermoacoustic Engine and Refrigerator". In *Acoustics 2009*. Adelaide, Australia, November, pp. 23–26.

Garrett, S.L., 2003. "Resource letter : TA-1 : Thermoacoustic engines and refrigerators". *Physics*, Vol. 72, No. 1, pp. 11–17.

Gentemann, A., Fischer, A., Evesque, S. and Polifke, W., 2003. "Acoustic Transfer Matrix Reconstruction and Analysis for Ducts with Sudden Change of Area". *9th AIAA/CEAS Aeroacoustics Conference and Exhibit, May 12-14, 2003, Hilton Head, South Carolina*, , No. May, pp. 1–11.

Guédra, M., Bannwart, F.C., Penelet, G. and Lotton, P., 2015. "Parameter estimation for the characterization of thermoacoustic stacks and regenerators". *Applied Thermal Engineering*, Vol. 80, pp. 229–237.

Higgins, B., 1802. "On the sound produced by a current of hydrogen gas passing through a tube". *Journal of Natural*

Philosophy, Chemistry, and the Arts, Vol. 20, No. 1, pp. 129—-131.

Junior, C.A.V., Bannwart, F.C. and David, S.A., 2017. "Fractional order calculus applied to generalize the Rott's linear thermoacoustics: an investigation toward energy regeneration in automobiles". In *24th ABCM International Congress of Mechanical Engineering*.

Noda, D. and Ueda, Y., 2013. "A thermoacoustic oscillator powered by vaporized water and ethanol". *American Journal of Physics*, Vol. 81, pp. 124–126.

Poese, M.E., 2017. *Handbook of Climate Change Mitigation and Adaptation*, Springer International Publishing Switzerland, Cham, Switzerland, chapter Thermoacoustics, pp. 2967–2994.

Rayleigh, J.W.S.B., 1896. *The theory of sound*, Vol. 2. Macmillan.

Rott, N., 1980. "Thermoacoustics". *Advances in Applied Mechanics*, Vol. 20, No. C, pp. 135–175.

Rott, N., 1969. "Damped and Thermally Driven Acoustic Oscillations inWide and Narrow Tubes". *Journal of Applied Mathematics and Physics (ZAMP)*, Vol. 20, No. 1, pp. 230–243.

Swift, G.W., 1988. "Thermoacoustic engines". *The Journal of the Acoustical Society of America*, Vol. 84, No. 4, pp. 1145–1180.

Swift, G.W., 2002. *Thermoacoustics: A Unifying Perspective for Some Engines and Refrigerators*, Vol. 1. Acoustical Society of America through the American Institute of Physics.

7. RESPONSIBILITY NOTICE

The following text, properly adapted to the number of authors, must be included in the last section of the paper: The author(s) is (are) the only responsible for the printed material included in this paper.